Proposal to Jefferson Lab PAC 19

Testing the Limits of the Full Relativistic $(\vec{e}, e'\vec{p})$ Reaction Model

F. Benmokhtar, S. Dieterich, R. Gilman, C. Glashausser[1], X. Jiang, G. Kumbartzki, R.D. Ransome[1], S. Strauch[1,*]
Rutgers University, Piscataway, NJ

E. Brash[1], G.M. Huber, A. Kozlov, G.J. Lolos, Z. Papandreou
University of Regina, Regina, SK

K. Wijesooriya
Argonne National Laboratory, Argonne, IL

C. Perdrisat
College of William and Mary, Williamsburg, VA

P.E.C. Markowitz
Florida International University, Miami, FL

L. Bimbot
Institut de Physique Nucléaire, Orsay, France

R. Ent, M.K. Jones, N. Liyanage, D. Meekins, S. Nanda, B. Wojtsekhowski
Jefferson Lab, Newport News, VA

V. Punjabi
Norfolk State University, Norfolk, VA

P. Ulmer, L. Weinstein
Old Dominion University, Norfolk, VA

A.J. Sarty
St. Mary's University, Halifax, Nova Scotia, Canada

J. Annand, D. Hamilton, D. Ireland, R. Kaiser, J. Kellie, K. Livingston, G. Rosner, D. Watts
University of Glasgow, Glasgow, Scotland, UK

J.J. Kelly
University of Maryland, College Park, MD

[1] Co-spokesperson
[*] Contact person

Abstract

We propose to measure the polarization transfer (P'_x and P'_z) and induced polarization P_y in the $^{16}\mathrm{O}(\vec{e},e'\vec{p})$ reaction at a Q^2 of 0.8 $(\mathrm{GeV/c})^2$. Recent measurements have shown that the full relativistic distorted wave impulse approximation model of Udias *et al.* could become a "standard model" for the $(e,e'p)$ reaction. The $^{16}\mathrm{O}(e,e'p)$ data from Jefferson Lab experiment 89-003 gave evidence of the need for full relativistic calculations which include dynamical enhancements of the negative energy components of the relativistic wave functions (spinor distortions). The conclusion is based primarily on a comparison of the measurements of A_{LT} at high missing momentum with the predictions of the Udias model. Because A_{LT} is not sensitive to spinor distortions at low missing momentum, this supplies only a limited test. The Udias calculations also provided a significantly improved description of polarization transfer data for $^4\mathrm{He}(\vec{e},e'\vec{p})^3\mathrm{H}$. The remaining discrepancies with the latter data provide a tantalizing indication of a possible modification of the nucleon form factors, in agreement with the density dependent form factor modifications predicted by a quark-gluon coupling (QMC) model of Lu *et al.* This finding needs to be explored further in a heavier nucleus.

The $^{16}\mathrm{O}(\vec{e},e'\vec{p})$ reaction provides both the denser nuclear environment and the sensitivity to spinor distortion at low missing momentum, where the reaction mechanism is better understood. Polarization observables are sensitive to the off-shell current operator and thus provide an excellent probe of medium-dependent form factors. The high precision data for several states with very small overall errors will provide a benchmark for comparison with theory.

The data of this experiment are a necessary complement to the cross section data E89-003 and the recently approved E00-102; together, they will provide the most extensive set of quasi-elastic electron scattering measurements on any complex nucleus. This measurement will provide a stringent test of both the best relativistic model available and of the QMC predictions for medium modification of the proton form factors. We request 27 days of beam time.

1. Physics Motivation

The high duty-factor, high polarization, and high current electron beams now available have made possible $(e, e'p)$ coincidence and polarization transfer measurements of unprecedented precision [1–6]. These new data allow much better tests of theoretical models of reaction mechanisms, and combined with a careful choice of kinematics, will allow one to isolate and study the many elements of models describing the reactions. Several interesting results have emerged from these recent experiments. Gao *et al.* [1] reported the first evidence of the need for full relativistic calculations, including distortion of the negative energy components of the wave function (spinor distortions), as shown in Fig. 1. Jones *et al.* [5] used polarization transfer to measure the G_E/G_M ratio for the proton with high precision and small systematic uncertainties, greatly improving on previous data and giving the completely unexpected Q^2 dependence of this ratio. Similarly, the first indication for a modification of the nucleon form factor in the nuclear medium using polarization transfer on ^{4}He was reported by Dieterich *et al.* [3]. The result was consistent with the prediction of a quark-meson coupling model (QMC) of Lu *et al.* [7], as shown in Fig. 2; the preliminary results of E93-049 [4] confirm the Mainz measurement. The ratio of the measured polarization transfer ratios from ^{4}He and ^{1}H, $R = (P'_x/P'_z)_{\rm He}/(P'_x/P'_z)_{\rm H}$, are compared to calculations by Udias *et al.* [8–10]. The plane-wave calculation serves as baseline. The full relativistic calculation predicts a reduced ratio, but cannot fully account for the measurement. The inclusion of the density dependent nucleon form factors from Lu *et al.* in the current operator leads the calculation at low Q^2 to good agreement with the data. Note the expanded scale in Fig. 2, which demonstrates the remarkable precision now available. Using the ratio cancels most systematic uncertainties of the experiment; beam polarization, luminosity, and analyzing power of the polarimeter all cancel in the ratio. Both Gao and Dieterich largely based their conclusions on the results of calculations of Udias who has, the most complete fully relativistic calculation using the mean-field approximation. However, his model does not yet include short range correlations (SRC), meson exchange currents (MEC), and isobar configurations (IC). The most recent calculation including those effects is the non-relativistic model of Ryckebusch [11]. Gao and Dieterich both estimated that the effects of SRC/IC/MEC were small. This estimate could be checked with additional measurements over a broader kinematic range.

The exciting results of both Gao and Dieterich demand more extensive measurements to unambiguously assess the effects of relativity and modification of the form factors. We will demonstrate how this can be done with high precision measurements of polarization transfer on ^{16}O. Polarization measurements test different aspects of models than cross section measurements do, and, since spin is intrinsically a relativistic phenomenon, one expects polarization observables will provide the best test of relativistic models. For example, the results of Gao are sensitive to spinor distortions only at rather high missing momentum; polarization observables would allow a test of the Udias calculation at low missing momentum. So, although the Udias model does a remarkably good job of explaining the existing data, more stringent tests of the model need to be made, and significant questions remain which can only be resolved with more data, and in particular with spin transfer observables.

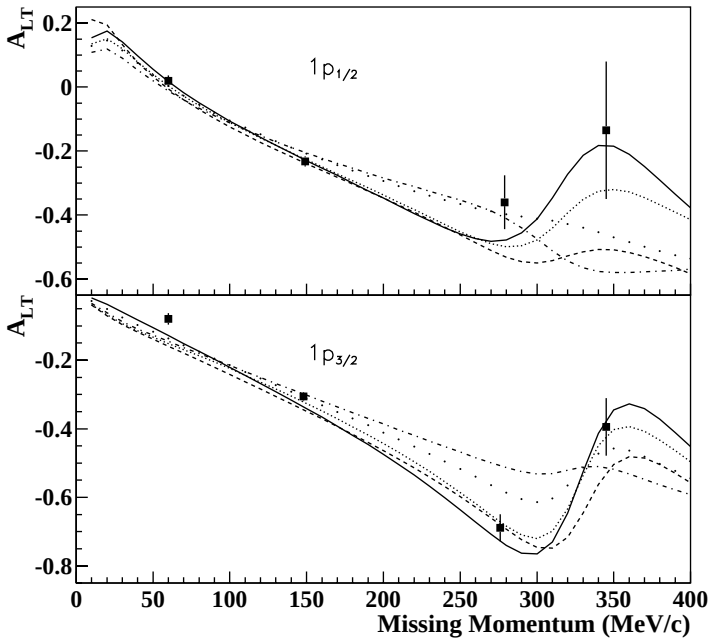

Figure 1. Measured left-right asymmetry A_{LT} for the ^{16}O$(e,e'p)$ reaction at $Q^2 = 0.8$ (GeV/c)^2 along with DWIA calculations from Kelly (dashed) [12] and Udias (all others) [9]; in particular a fully relativistic calculation (solid) and calculations with no spinor distortions (dotted-dashed), only bound-state spinor distortions (densely dotted), and only ejectile spinor distortions (loosely dotted) included. Figure taken from Ref. [1].

- The existing ^{16}O data of R_{LT} and A_{LT} are sensitive to distortions of the bound state spinor, but insensitive to spinor distortions of the recoil particle. Spin transfer observables are sensitive to recoil spinor distortions at low missing momentum, where the reaction is better understood, and provide a much more complete test of any model.

- The combination of Mainz and JLab data on ^{4}He at low Q^2 gives a statistically significant deviation from calculations that do not include a form factor modification. A confirmation of the ^{4}He result in another nucleus where the density dependence of possible modifications can be studied by the knockout from different shells is essential. The previous oxygen cross section measurements are insensitive to modifications of the form factor, while spin observables are sensitive to modifications.

We are proposing here an experiment aimed at answering the above questions. Measurements of polarization transfer on ^{16}O at a Q^2 of 0.8 (GeV/c)^2 would complement the ^{16}O$(e,e'p)$ cross section data from E89-003 [15] and its proposed update, E00-102 [16], giving the most extensive set of measurements on any complex nucleus. We will also provide high-precision data for the $1s_{1/2}$ shell, which can be then compared to the

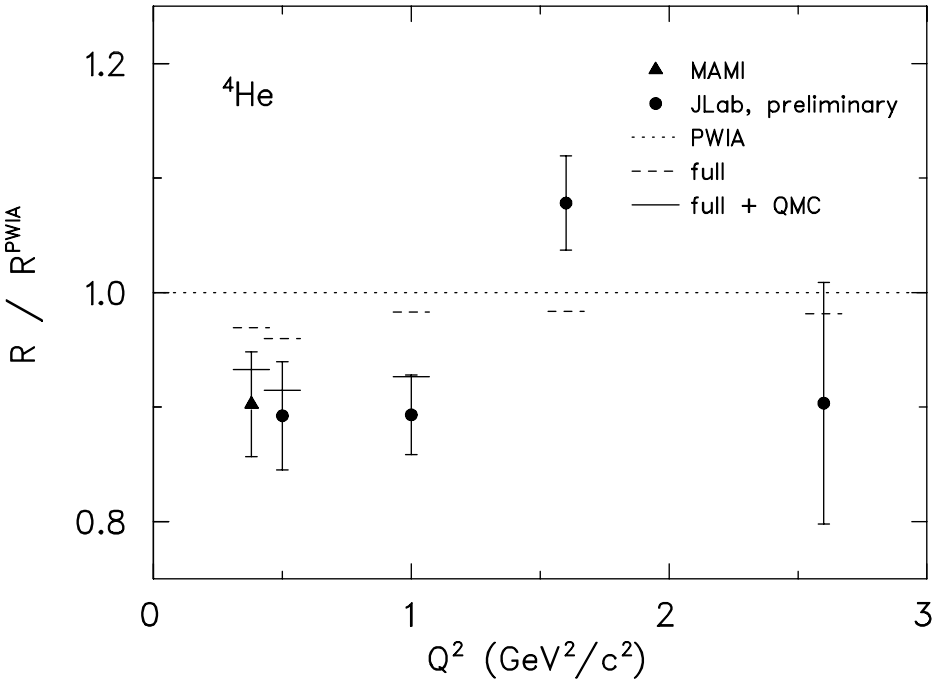

Figure 2. Measured values of the double ratio of polarization transfer observables $R = (P'_x/P'_z)_{\rm He}/(P'_x/P'_z)_{\rm H}$ for the ^{4}He$(\vec{e},e'\vec{p})$ reaction from Mainz [3] and, preliminary, JLab E93-049 [4]. The theoretical curves represent plane-wave calculations (dotted) and fully relativistic DWIA calculations (dashed and solid) from Udias. The solid line use a modified current operator in which nucleon form factors depend upon local density as predicted by Lu *et al.* [7]; in their present form the latter calculations are applicable for $Q^2 \leq 1$ (GeV/c)^2 [13]. Errors are dominated by statistical uncertainties.

existing results for ^{4}He. The previous polarization measurement on ^{16}O, E89-033 [14], was a commissioning experiment and did not obtain sufficient statistical precision to help decide these issues.

The measurements of the ratio of transfered polarizations and of the induced polarization for different states, for several values of both positive and negative missing momentum with good statistical precision will play a key role in determining the need for relativity in the standard nuclear model and the presence of medium modifications of nucleon properties. In addition, we will measure in a kinematic region dominated by single particle knockout where the cross sections are large and theoretical uncertainties are expected to be smallest. By using the ratio of transferred polarizations we also eliminate most experimental systematic uncertainties. These points will be discussed in detail below.

2. Proposed measurement

2.1. Kinematics

We propose to measure the recoil polarization of the outgoing protons in the $^{16}\mathrm{O}(\vec{e},e'\vec{p})$ and $^{1}\mathrm{H}(\vec{e},e'\vec{p})$ reaction at $Q^2 = 0.8$ (GeV/c)^2. We will use a beam energy of 2.4 GeV, the same as E89-003 to make the closest comparison with the cross section measurement. This beam energy also provides a balance between the count rate and the magnitude of the transfered polarization. A beam energy as low as 1.6 GeV could be used without a significant decrease of the relative uncertainty of the polarization transfer measurement, although induced polarization uncertainties would increase. We will make two measurements in quasi-perpendicular kinematics, with the emphasis on the single particle knockout from the $1p_{1/2}$ and $1p_{3/2}$ states, and one in parallel kinematics at low missing momentum, where the sensitivity to the $1s_{1/2}$-shell knockout is highest. The measurements will concentrate on the region of small missing momentum and in quasi-elastic ($Q^2/2m_p \approx \omega$) kinematics, where theoretical uncertainties are expected to be smallest. Figure 3 shows the reaction coordinate system. Elastic $\vec{e}p$ scattering data will also be taken. In order to determine the polarization double ratio, R, the hydrogen ratio must be determined with a statistical precision comparable to the oxygen ratio. By determining the hydrogen polarization ratio with the same experimental setup as the oxygen ratio systematic uncertainties in the spin transport can be largely eliminated. In addition the hydrogen data can be used to determine the instrumental asymmetries in the polarimeter, which is needed to make a precise measurement of the induced polarization. Table 1 summarizes the proposed kinematics, values are given for the central setting, where E and E' are the incident and final electron beam energy, p_p is the momentum of the recoil proton, θ_e and θ_p are the electron and proton angles relative to the beam axis, and $\Delta\theta_{pq}$ is the proton angle relative to the three momentum transfer axis.

Table 1
Kinematics for the proposed $^{16}\mathrm{O}(\vec{e},e'\vec{p})$ and $^{1}\mathrm{H}(\vec{e},e'\vec{p})$ measurements.

Kin	Target	Q^2	E	E'	θ_e	p_p	θ_p	$\Delta\theta_{pq}$
		(GeV/c)^2	(GeV)	(GeV)	(deg)	(GeV/c)	(deg)	(deg)
A	^{16}O	0.8	2.442	2.003	−23.4	0.978	47.8	−5
B	^{16}O	0.8	2.442	2.003	−23.4	0.978	57.8	5
C	^{16}O, ^{1}H	0.8	2.442	2.003	−23.4	0.978	52.8	0

In the following section we will discuss the predictions of the models of Udias and Ryckebusch, and how the combination of measurements proposed will restrain the models significantly more than existing measurements. The main issues we will address are: the need for relativistic dynamical effects (spinor distortions) and medium modification of the proton form factor, as predicted by Lu *et al.* The discussion will first deal with the p-shell states, then with the s-state calculations afterward.

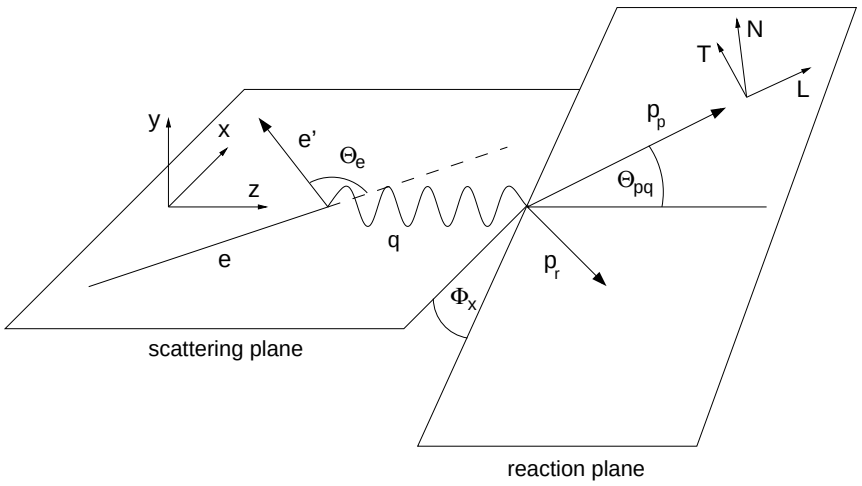

Figure 3. Kinematics for the ^{16}O$(e,e'p)$ reaction showing the electron scattering plane, the reaction plane and two coordinate systems in which polarization of the protons is expressed.

2.2. Theoretical Expectations

2.2.1. Relativity

The full relativistic calculations of Udias *et al.* provide excellent descriptions of the left-right asymmetry, A_{LT}, and longitudinal-transverse interference response function, R_{LT}, for the $1p$-shell knockout in ^{16}O$(e,e'p)$ [1]. Relativistic dynamical effects are required to describe the data. These effects are mainly visible at high missing momenta, where the cross sections are small and several other nucleus related effects may play a role. Moreover the investigation of the $1p_{3/2}$ knockout at high missing momentum is complicated by the presence of other states ($2s_{1/2}$, $1d_{5/2}$, and $1d_{7/2}$, see e.g. Ref. [17]), which have a total cross section about equal to that of the $1p_{3/2}$ state at $p_m > 330$ MeV/c. These were unresolved in Ref. [1] and have to be accounted for. There is also an unexplained statistically significant deviation in A_{LT} at a missing momentum of about 60 MeV/c.

Measurement of the polarization observables will determine the role of spinor distortions at low missing momentum. Here, at the maximum of the cross section for p shell knockout, the cross section contribution from unresolved states is minimal (as will be shown later in Table 5) and the sensitivity to relativistic effects and the interpretation of the data is cleaner. Figure 4 shows the ratio of the polarization transfer observables for proton knockout from the $1p_{1/2}$ and $1p_{3/2}$ states of ^{16}O as a function of missing momentum. All calculations were done with the Udias code with the same input as in Ref. [1]. We plot the fully relativistic result obtained with the $cc1$ (dash-dotted) and $cc2$ (dashed) de Forest [18] current operators and compare these with results where the negative-energy components of the bound state and ejectile wave functions are projected out. The differences between the full and projected calculations are due to the dynamical enhancement of the lower components [9]. The effect of this is a reduction of the polarization ratio well within the

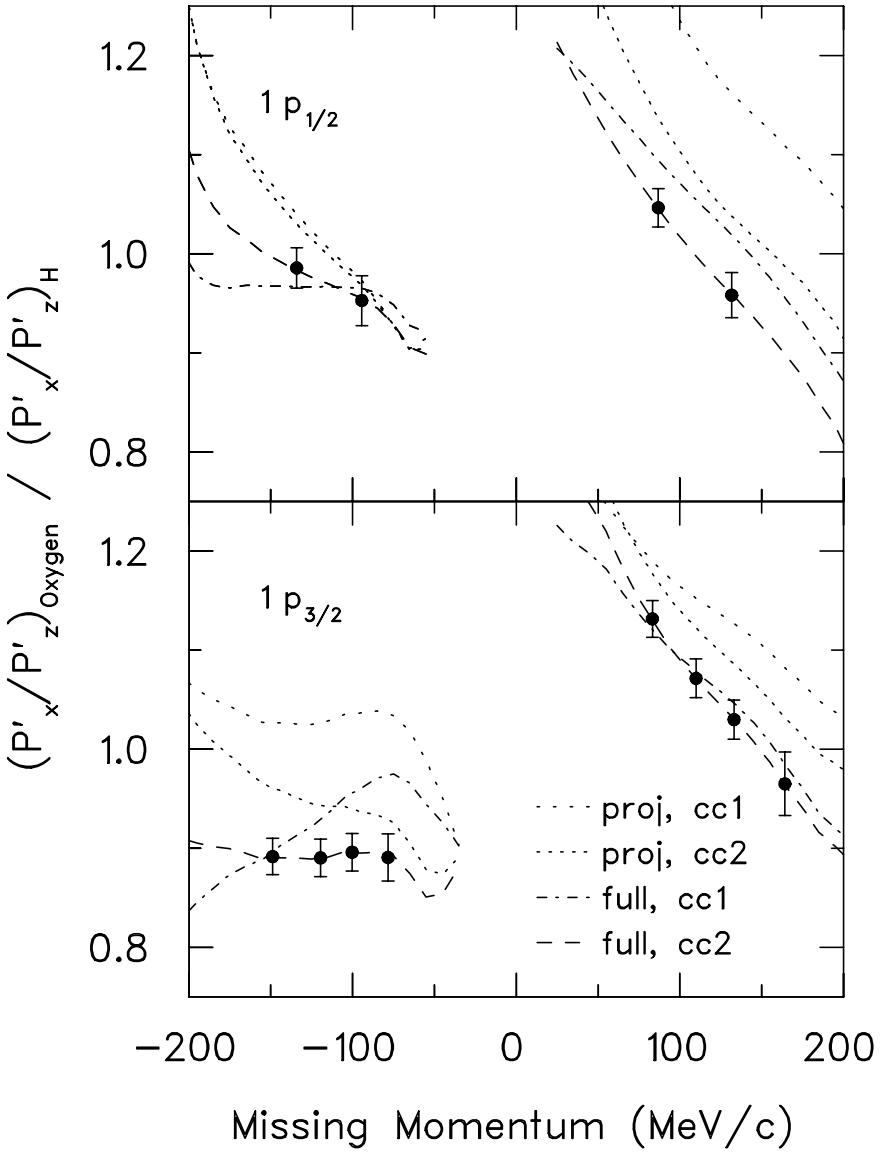

Figure 4. Polarization ratio for proton knockout from the $1p_{1/2}$ and $1p_{3/2}$ states of ^{16}O as a function of missing momentum. Calculations are from Udias for the positive energy projection and full calculation, and for the $cc1$ and $cc2$ current operator. Sample data points with the anticipated errors for the proposed experiment are shown on the full calculation using the $cc2$ current operator; data points with $p_m < 0$ correspond to kinematics A, data points with $p_m > 0$ to kinematics B.

experimental sensitivity. It was shown in [10] that the $cc1$ current operator gives more weight to the dynamical enhancement of the lower components than $cc2$. Experiment 89-003 found a slightly better description of their cross section data with the $cc2$ current operator, whereas the analysis of the Mainz ^{4}He polarization data fit more to the $cc1$ operator, with its lower predictions of the polarization ratio. The problem of the off-shell current operator can only be addressed in an attempt to consistently and simultaneously describe the high precision data from cross section and polarization experiments.

The normal component of the induced polarization P_y is identically zero assuming one-photon exchange and no FSI between the ejected nucleon and the residual system. Hence, any observed deviation from zero is an indication of FSI. Moreover, model assumptions on optical potentials are constrained through P_y. The induced polarization is predicted to be substantial and shows sensitivity to relativistic effects. For the $1p_{3/2}$ shell, shown in Fig. 5, and $p_m < 0$ there are small Gordon ambiguities and a very clear separation of the fully relativistic calculation results from the projected ones is seen. The induced polarization is insensitive to possible medium modifications of the nucleon form factors.

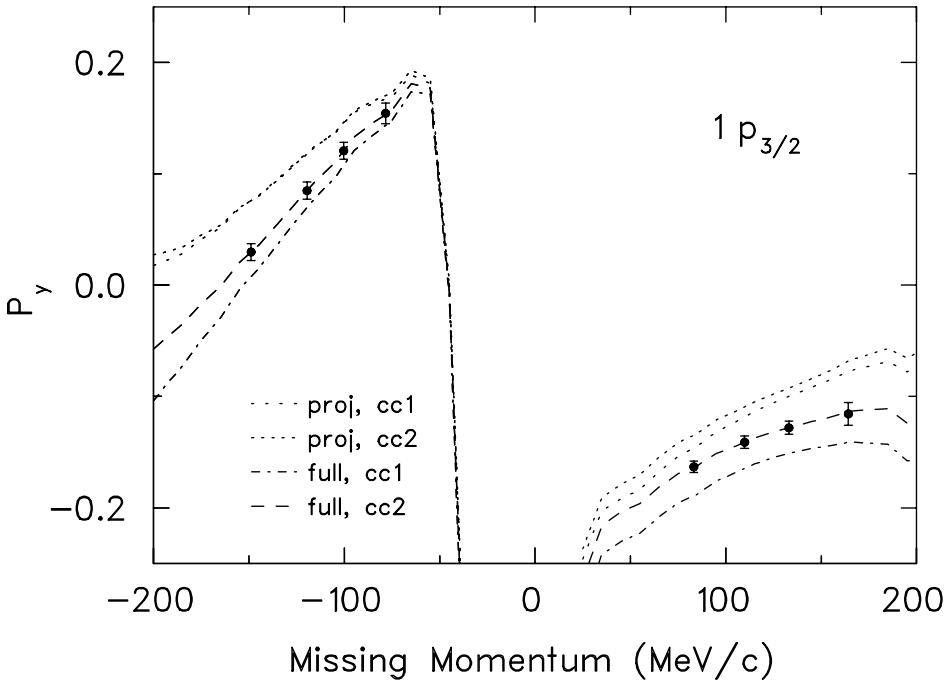

Figure 5. The induced polarization P_y for the $^{16}\mathrm{O}(\vec{e},e'\vec{p})^{15}\mathrm{N}(1p_{3/2})$ reaction at $Q^2 = 0.8$ (GeV/c)^2. Calculations are from Udias for the positive energy projection and full calculation, and for the $cc1$ and $cc2$ current operator. Sample data points with the anticipated errors for the proposed experiment are shown on the full calculation using the $cc2$ current operator.

2.2.2. Two-body currents

Two-body contributions may complicate the interpretation of double polarization observables in terms of medium dependent nucleon form factors. The very good description

of the ^{16}O$(e,e'p)$ cross section data [1] with the Udias full relativistic DWIA calculation, which does not include MEC and IC contributions, was interpreted as evidence that these contributions are not important up to p_m of 345 MeV/c.

Although two-body current effects are not well studied in finite nuclei, the latest calculations of Ryckebusch [11] do indicate that MEC and IC will have a measurable effect on spin observables, and that the effects will be measurably different for different angular momentum states. Figure 6 shows the polarization transfer ratio for $1p_{1/2}$ and $1p_{3/2}$ knockout predicted by Ryckebusch, normalized to a calculation not including two-body effects. The striking feature is that the combined effect of MEC and IC is predicted to be very large (nearly 20%) in the $1p_{3/2}$ state and for negative missing momentum, but not the $1p_{1/2}$. Within this model, a substantial deviation from the DWIA calculation only for this region would be a clear signature of MEC+IC effects. The group of Udias is working to include the MEC and IC into the full relativistic calculation [20]. The proposed measurement will provide a benchmark for future improvements in these models.

This is another excellent example of how by looking at the same polarization observable in different nuclear states, and at positive and negative recoil momentum, we are able to distinguish between the various contributing physical processes.

2.2.3. Medium modification of proton form factor

There have been numerous predictions that the proton form factor will be modified by the nuclear medium [7,21–24]. Previous measurements of cross sections have limited the change to a few percent for the magnetic form factor and about 10% for the electric form factor [17,25–31]. The predicted modifications in most models are consistent with the existing data. However, the form factor of a bound nucleon is not directly observable; it must be inferred from calculations which predict how a modification of the form factor will affect measurable quantities such as cross sections or polarizations. The ratio of the polarization transfer observables are particularly sensitive to a possible medium modification. This can be seen from electron-nucleon scattering, where there exists a direct relationship between the ratio of the electro-magnetic form factors, G_E/G_M, and the polarization components [32]:

$$\frac{G_E}{G_M} = -\frac{P_x}{P_z} \cdot \frac{E+E'}{2m_N} \tan(\theta/2) \qquad (1)$$

This relationship is only approximately correct for electron scattering from a bound nucleon; one must calculate the expected polarization ratio in the context of some model. Taking full advantage of the constraints on models by E89-003 and after understanding possible two-body effects in the reaction with the help of the polarization data, an observation of further deviations of the data from the full calculation would point to medium modifications of the proton form factor.

Figure 7 shows the polarization double ratio predicted by the full calculation including the medium modified form factors by Lu *et al.* relative to the ratio predicted by the full calculation employing the free form factor. The medium modification was included by replacing the free form factors in the current operator by medium modified ones. The expected effect is density dependent and therefore significantly different between the p-shell and s-shell knockout, as will be shown later. This variation (5% to 12%) provides much tighter constraints to investigate medium effects than the single s-shell knockout

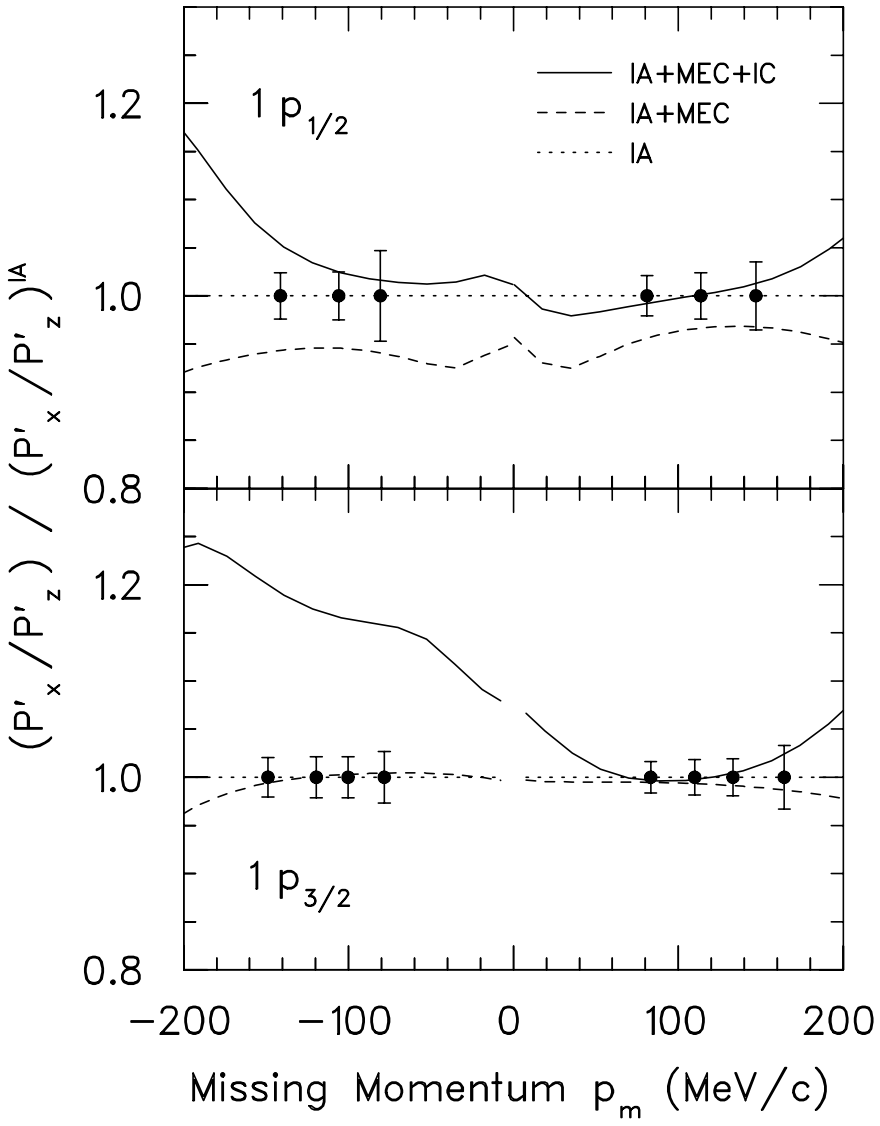

Figure 6. Polarization ratio (P'_x/P'_z) for the $^{16}\mathrm{O}(\vec{e},e'\vec{p})$ reaction at $Q^2 = 0.8$ (GeV/c)^2 relative to the ratio $(P'_x/P'_z)^{\mathrm{IA}}$ when solely one-body currents are retained in the calculation; The dotted curve shows the result for the impulse approximation; in the dashed curve MEC effects are also included, and the solid curve represents the full calculation including also IC. Theoretical results are by Ryckebusch Ref. [11,19]. Sample data points with anticipated errors for the proposed experiment are shown.

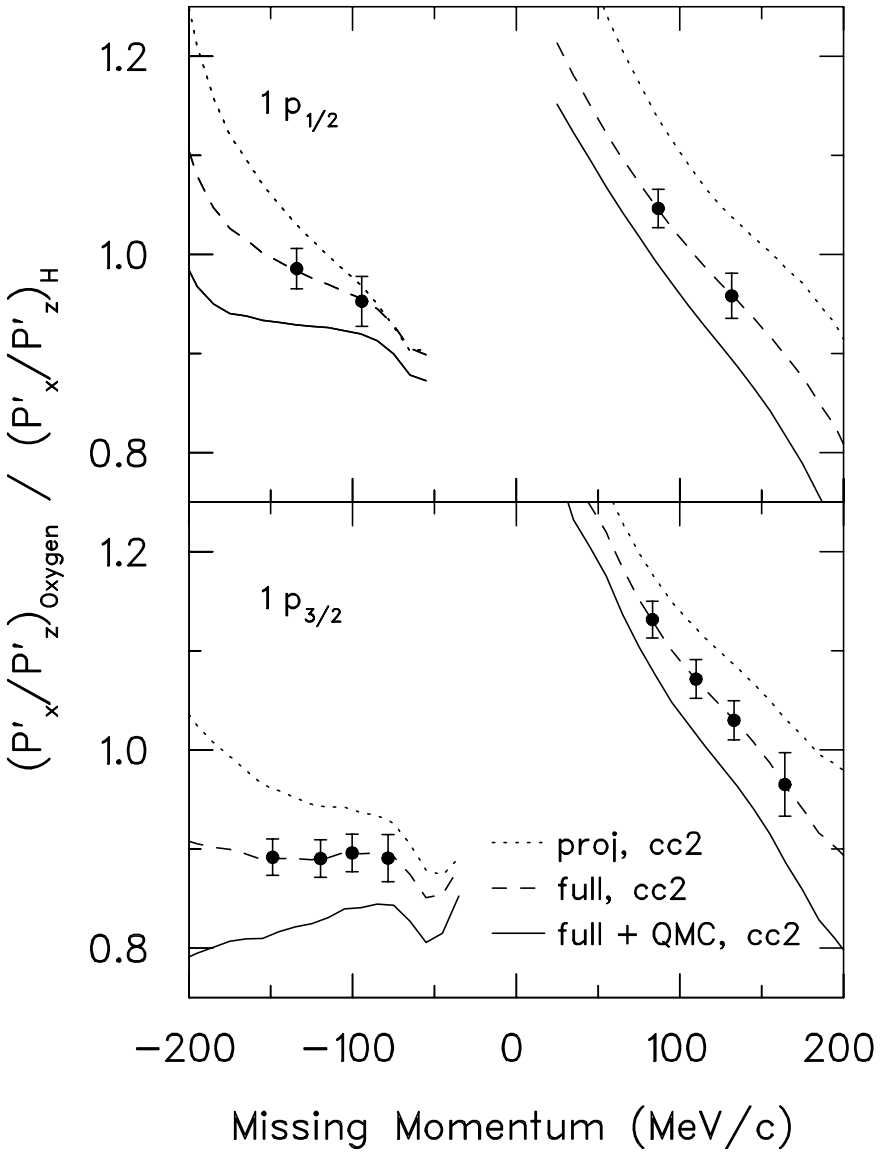

Figure 7. Polarization ratio from Udias for the positive energy projection (dotted), full calculation (dashed), and the full calculation including density dependent nucleon form factors predicted by Lu *et al.* [7] (solid). Sample data points with the anticipated errors for the proposed experiment are shown on the full calculation using the *cc*2 current operator.

in ^{4}He. The effect of QMC is to lower the ratio in all states and for both positive and negative missing momentum.

2.2.4. Proton knockout from the s-shell

As we have shown above, p-shell knockout alone should be sufficient to resolve the physics questions discussed in the introduction. In principle, s-shell knockout provides the best test for density dependence of the form factor. Ryckebusch also predicts large effects from MEC/IC in the s-shell. However, interpretation of the results relies on being able to isolate the single particle knockout component in the higher missing energy region. Thus, we will use missing energy only up to 40 MeV, and missing momentum below 100 MeV/c, where we expect the reaction to be dominated by single particle knockout, as shown by the calculations of Kelly, reported in Ref. [2]. Because the predicted effects on the polarization are so large, as shown in Fig. 8, s-shell knockout will provide an important consistency test.

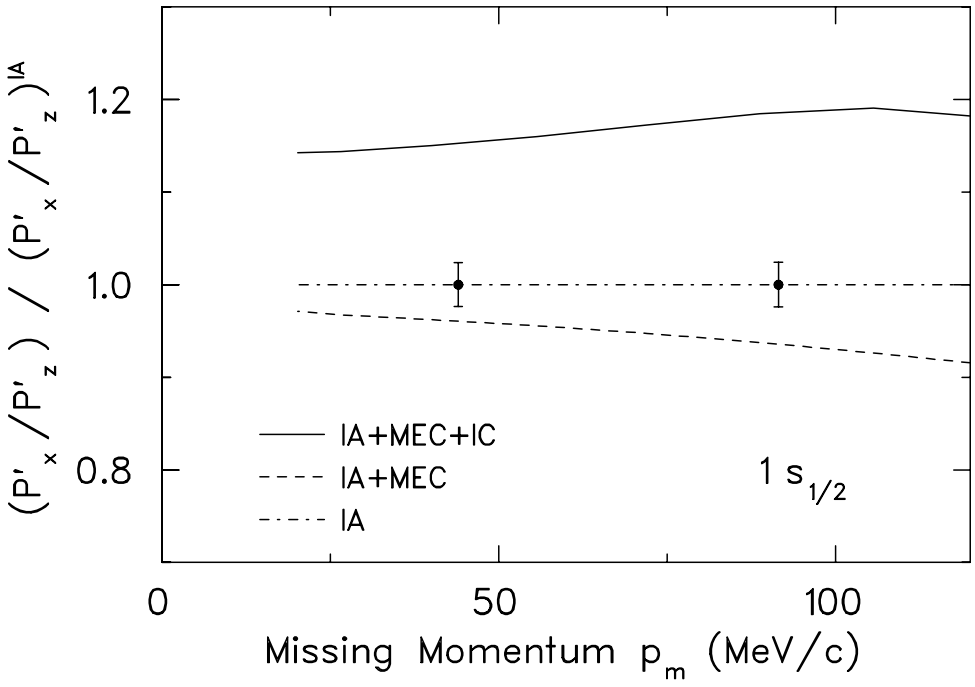

Figure 8. The same calculations as in Fig. 6 but for knockout from the $1s_{1/2}$ orbit. Sample data points with anticipated errors for the proposed experiment are shown.

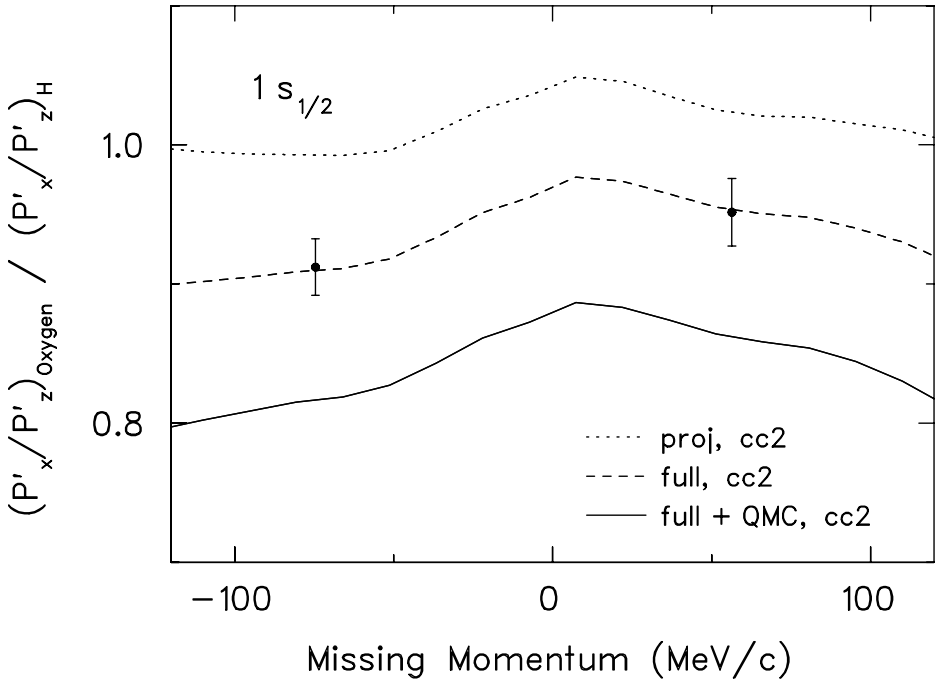

Figure 9. Estimated polarization transfer double ratio for the $^{16}\mathrm{O}(\vec{e}, e'\vec{p})^{15}\mathrm{N}(1s_{1/2})$ reaction as a function of missing momentum for the proposed $Q^2 = 0.8$ (GeV/c)^2 kinematics along with anticipated data points. The calculations were done with Udias code, $cc2$ current operator, and are fully relativistic (dashed), negative energy components projected to positive energy (dotted), fully relativistic including QMC medium modified form factors (solid).

3. Apparatus

3.1. Overview

The experiment is proposed for Hall A at Jefferson Lab. The experiment will make use of the two large solid angle high resolution spectrometers (HRS). An incident 75% polarized electron beam with beam currents up to 80 μA and energy of 2442 MeV will be used. With the exception of a liquid oxygen target, the proposed experiment will only employ the usual Hall A equipment. Both spectrometers will be equipped with their standard detector systems.

3.2. The liquid ^{16}O target

Previous oxygen experiments have used a waterfall target. Our desired statistical accuracy demands a higher luminosity than is available with the current waterfall target if we are to keep the running time reasonable. Assuming the beam current is limited to about 80 μA, an increase of the target thickness is the only way to gain luminosity. Equally important, the hydrogen content of the waterfall target makes measurements in the proposed parallel kinematics impractical. We therefore propose to build a new liquid oxygen target. The target we are proposing is of cylindrical shape with the beam crossing the target on a diameter. This robust design offers the advantage of construction simplicity; its fabrication is straightforward. Some of its characteristics are summarized in Table 2, in part inspired by properties of the existing ^{4}He high pressure cryogenic gas target. The transverse flow of the liquid oxygen through the whole target volume maximizes flow velocity through the beam region and cooling of the target walls. Running a thick, liquid cryogenic target with high beam currents raises technical, safety, and data-analysis issues which we will address in the following.

Table 2
Characteristics of the planned liquid oxygen target

Nitrogen boiling point	77.36 K
Oxygen boiling point	90.18 K
Oxygen melting point	54.75 K
Density of liquid oxygen	1.141 g/cm^3
Oxygen radiation length	32.24 g/cm^2
Cell diameter	2.0 cm
Cell wall thickness	0.033 cm
Target thickness	2.28 g/cm^2
Dissipated power	$\approx$ 500 W for a 80 μA beam

a) **Technical issues.** The power dissipated in the ^{16}O target is 500 W for a 80 μA beam. Since oxygen has a higher boiling point than nitrogen there is no technical concern in providing the necessary cooling power. A LN2 cooling line will have to

be made. We are not very sensitive to boiling effects; they reduce the luminosity, but we are not sensitive to the absolute luminosity. Liquid hydrogen targets have been successfully run at JLab with equally high currents for some years and oxygen presents fewer cooling problems. The higher density of oxygen will require different fans for circulation than the ones used for hydrogen.

b) **Safety issues.**

The target has a thickness of 7% in terms of radiation length and a tolerable radiation load similar to that of E00-003 with its 10% radiation length ^{208}Pb target and 50 μA.

c) **Data analysis issues.**

With a target length of 2 cm the entry and exit windows of the target cell will be fully visible within the spectrometer acceptances. The vertex resolution of the spectrometers is not high enough to separate out completely scattering events from the windows without reducing the usable target length to an unacceptable low level. Assuming a total entry plus exit window thickness of 0.17 mm, the rate coming from the aluminum windows relative to oxygen scatterers is approximately $(Z\rho x/A)_{^{27}\mathrm{Al}}/(Z\rho x/A)_{^{16}\mathrm{O}}$ and is less than 2%.

The thickness of the target will cause the energy loss to be smeared out over 6-8 MeV. However, the location of the scatter is known to about 2 mm. By correcting for the energy loss, a resolution of better than 2 MeV can be obtained, well below that needed to separate the $1p_{1/2}$ from the $1p_{3/2}$ state.

4. Count Rate and Running Time Estimates

4.1. Count rate estimates

The ^{16}O$(e,e'p)$ cross sections have been estimated with response functions from the fully relativistic DWIA code of Udias. The calculations used the same input as in Ref. [1]. These include the EDAIO optical model of Cooper *et al.* [33], NLSH bound-state wave functions [34], the Coulomb gauge, and the *cc*2 off-shell current operator. The response functions were used in the latest version of the Monte Carlo code for electro-nuclear coincidence experiments (MCEEP) [35] to calculate the cross section averaged over the experimental acceptance. Table 3 gives an overview of the ^{15}N-states included in the estimates, these are the prominent $1p_{1/2}$ and $1p_{3/2}$ hole states and the $(2s_{1/2}, 1d_{5/2})$ doublet which will not be separable from the $1p_{3/2}$ state. The $1s_{1/2}$-state lies in the continuum. Its missing energy distribution was estimated by spreading the cross section using the Lorentzian shape of Ref. [36]. This is the dominant part of the cross section at low missing momentum. For $p_m > 200$ MeV/c the cross section is dominated by a flat cross section contribution which is not attributed to single-nucleon knockout [2]. This additional strength was neglected in the cross section estimates for this proposed measurement which has an average p_m of about 70 MeV/c for the *s*-shell knockout.

Table 3
States of ^{15}N included in the estimation of the cross section and polarization observables for the ^{16}O$(\vec{e},e'\vec{p})$ reaction along with excitation energy in ^{15}N and spectroscopic factors.

State	E_x (MeV)	S	Ref.
$1p_{1/2}$	0.00	0.73	[1]
$1d_{5/2}$	5.27	0.090	[37]
$2s_{1/2}$	5.30	0.034	[37]
$1p_{3/2}$	6.32	0.71	[1]
$1s_{1/2}$	≈ 28	0.73	[2]

Count rates were calculated from the ^{16}O$(e,e'p)$ and ^{1}H$(e,e'p)$ cross sections using the MCEEP model of the Hall A HRS spectrometers with their open collimator configuration. Radiative effects and the energy loss in the targets were taken into account. Table 4 summarizes the count rate estimates for oxygen. The hydrogen rate will be limited by the data acquisition system; we assume a rate of 1800 events per second.

The data will be analyzed in three missing mass bins where the single proton knockout from the $1p_{1/2}$, $1p_{3/2}$ and $1s_{1/2}$ shells dominates. The missing mass resolution of about 2 MeV does not allow for a separation of less dominant states. These and the radiative tail from low lying states establish a background contribution to the dominant strength in the respective missing mass bin. These contributions were included in the cross section and polarization estimates. Figure 10 illustrates this and shows the estimated missing mass distribution for parallel kinematics. The total event distribution (solid curve) is shown along with three differently hatched areas corresponding to the knockout from the three

Table 4
Anticipated $(e,e'p)$ cross sections and coincidence rate for the three proposed kinematical setting with $Q^2 = 0.8$ (GeV/c)^2 assuming an ^{16}O target density of 2.28 g/cm^2 and electron beam current of 80 μA.

Kin	Cross section (nb/MeV/sr^2)				Rate (1/s)				
	$1p_{1/2}$	$(2s,1d)$	$1p_{3/2}$	$1s_{1/2}$	$1p_{1/2}$	$(2s,1d)$	$1p_{3/2}$	$1s_{1/2}$	total
A	1.23	0.09	1.96	1.28	117	8	176	116	417
B	1.74	0.13	2.97	1.32	155	12	265	119	551
C	1.44	0.19	2.04	2.36	130	18	181	213	542

different shells. The bars on top indicate regions where the contribution of the knockout from the respective shell is larger than the summed contribution of the others, region (3) is restricted to a maximum missing mass of 40 MeV. The considered energy ranges and the expected background are given in Table 5. It shows that the yield contribution from the unresolved $(2s,1d)$ doublet is negligible.

Table 5
Missing mass regions. Estimations of yield contributions include energy resolution and radiative tail. Note, no $p_m < 100$ MeV/c cut is applied here for the s-shell, its inclusion would reduce background contributions in this region (3) by about a third.

Region	Missing mass (MeV)	Kin	Yield contribution (%)			
			$1p_{1/2}$	$(2s,1d)$	$1p_{3/2}$	$1s_{1/2}$
(1)	-2.5 – 4.5	A	99	1	0	0
		B	99	1	0	0
(2)	5.0 – 20.0	A	14	3	83	0
		B	12	3	85	0
(3)	26.5 – 40.0	C	7	1	12	80

Single rates from the (e,e'), (e,π^-), (e,p) or (e,π^-) reaction cause accidental coincidences which are a source of background for ^{16}O$(e,e'p)$. The single rates were estimated with the MCEEP code and its implementation of the routines of Lightbody and O'Connell [38] and are listed in Table 6. The coincidence time resolution is about 1 ns. The anticipated accidental coincidence rates within that time are also given in Table 6 and are small compared with the true coincidence rates listed in Table 4, and most will be eliminated after applying kinematical cuts. The total anticipated trigger-rate for the three measurements on oxygen, assuming a trigger coincidence time of 50 ns is given in Table 7 along with the respective estimated data acquisition dead time. This dead time was applied for the estimate of the required beam time.

Table 6
Anticipated single and accidental coincidence rates for the three proposed kinematical settings with $Q^2 = 0.8$ (GeV/c)^2 assuming a ^{16}O target density of 2.28 g/cm^2 and electron beam current of 80 μA. The accidental rate is given for a coincidence time resolution of $\Delta\tau = 1$ ns.

Background single rates (10^3/s)				
Kin	(e,e')	(e,π^-)	(e,p)	(e,π^+)
A	95	20	220	40
B	95	20	32	35
C	95	20	132	38
Accidental coincidence rates ($\Delta\tau = 1$ ns) (1/s)				
Kin	$(e,e'p)$	$(e,e'\pi^+)$	(e,π^-p)	$(e,\pi^-\pi^+)$
A	20.9	3.8	4.4	0.8
B	3.0	3.3	0.6	0.7
C	12.5	3.6	2.6	0.8

Table 7
Anticipated total trigger rate and data acquisition dead time. The total trigger rates include true and accidental coincidences assuming a coincidence time of 50 ns for the three proposed kinematical settings with $Q^2 = 0.8$ (GeV/c)^2 and a ^{16}O target density of 2.28 g/cm^2 and electron beam current of 80 μA.

Kin	Rate (1/s)	Dead time (%)
A	1920	20
B	950	10
C	1540	15

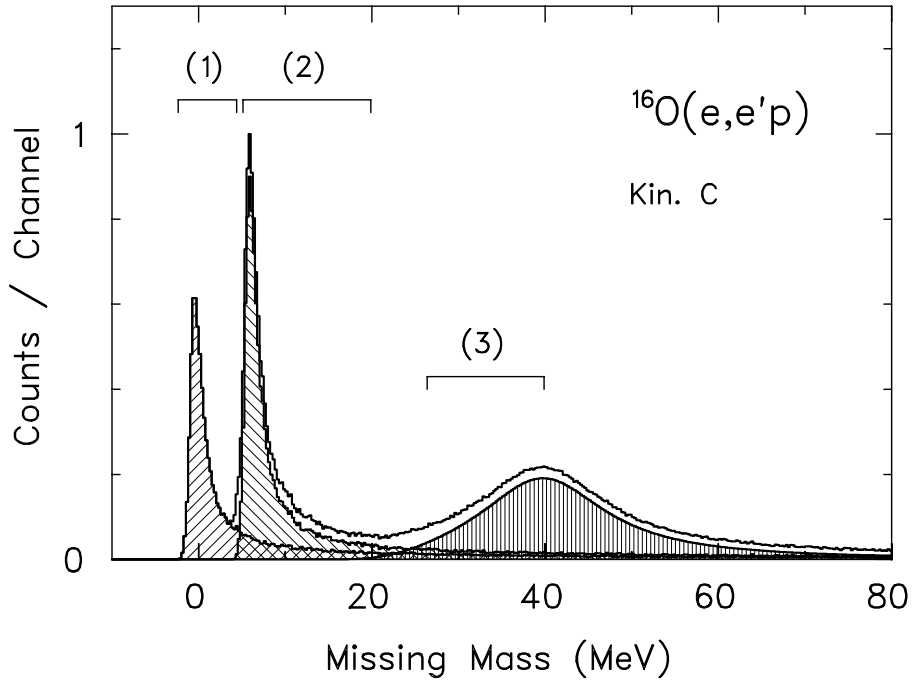

Figure 10. Monte Carlo simulation of the $^{16}\mathrm{O}(e,e'p)$ missing mass distribution for the proposed kinematics C at $Q^2 = 0.8$ (GeV/c)^2. The bars labeled (1), (2), and (3) indicate the regions corresponding to mainly $1p_{1/2}$, $1p_{3/2}$ and $1s_{1/2}$ shell knockout, respectively.

4.2. Polarization predictions

The cross section weighted polarization observables were estimated with the MCEEP code and Udias response functions. The acceptance averaged polarization components were expressed in the (x, y, z) basis, where $\hat{z}$ is along the three momentum transfer and $\hat{y}$ is normal to the electron scattering plane, and $\hat{x} = \hat{y} \times \hat{z}$, see Fig. 3. The background from lower lying states in each of the three missing momentum regions was properly taken into account in the estimation. Figure 11 shows the small dilution effect of the background on the polarization double ratio. The dashed curves assume a pure, single-shell contribution in each region. The solid curves have background contributions included. For the first region, where only $1p_{1/2}$ knockout occurs, both curves overlap. In the yield maximum the largest effect is seen for the $1p_{3/2}$ region at negative missing momentum where the polarization double ratio is decreased by 1.5%.

The absolute statistical uncertainties in the two accessible polarization components in the polarimeter frame, P_x^{FPP}, and P_y^{FPP} are

$$\Delta P = \frac{1}{\bar{A}_c}\sqrt{\frac{2}{\epsilon N_0}} \tag{2}$$

where $\bar{A}_c$ is the analyzing power averaged over an angular cone for which A_c is substantially different than zero, ϵ is the number of events which scatter into this cone and N_0 is the total number of events detected in the spectrometer focal plane. The polarizations

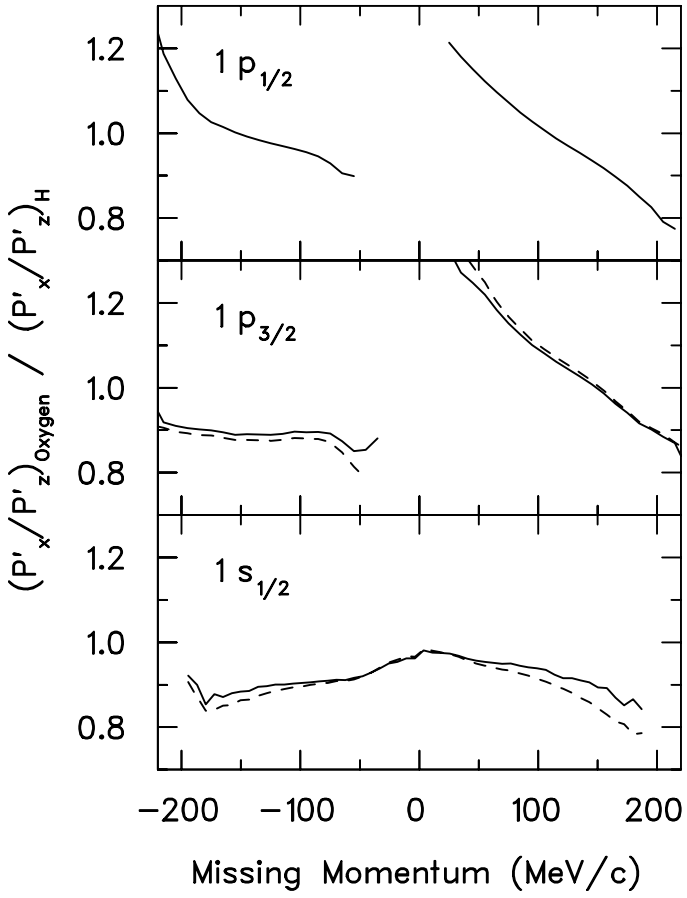

Figure 11. Estimations of the ^{16}O to hydrogen polarization double ratio using the Udias full calculation. The dashed lines show the predictions for the three different hole states; the solid lines include the diluting effects of the background in the three different missing mass regions.

in the polarimeter basis are linear functions of the proton's polarization components at the target. The relationship is given by a rotation which takes into account the change of coordinate system and the proton spin precession in the spectrometer's magnetic fields. For the estimation of the expected statistical uncertainties on the polarization observables a simplified spin transport was used

$$P_y^{\mathrm{FPP}} = P_y \cos\chi + hP'_z \sin\chi \quad (3)$$

$$P_x^{\mathrm{FPP}} = hP'_x \quad (4)$$

Here h is the electron beam polarization. The precession angle χ through the spectrometer

$$\chi = \frac{g_p - 2}{2}\,\gamma\,\Omega_B \quad (5)$$

is expressed in terms of the Lorentz factor γ, the proton g-factor, and the net bend angle of the trajectory through the spectrometer $\Omega_B = 45°$. Table 8 summarizes the assumed polarimeter and spin transport parameters.

Table 8
Assumed polarimeter- and spin transport parameters. the values of $\bar{A}_c$ and ϵ are taken from [39].

Kin	p	$\bar{A}_c$	ϵ	h	χ
A – C	978 (MeV/c)	0.364	0.082	75%	116.5°

4.3. Systematic uncertainties

The estimate of systematic uncertainties in the determination of the polarization observables and the polarization ratio is based on the experiences from other Hall A polarimeter experiments. The main systematic uncertainty is the determination of the spin transport of the proton in the spectrometer. Radiative effects are expected to be of order 1% [40]. For experiment 93-027 [5] the estimated systematic uncertainties on the polarization ratio (P'_x/P'_z) for settings close to the proposed ones were than 0.02. The analysis of the MAMI ^{4}He$(\vec{e},e'\vec{p})$ experiment showed that the systematic uncertainties on the polarization double ratio are largely decreased if the oxygen and hydrogen polarization ratio is measured within the same experiment and setting [3]. We expect systematic uncertainties on the polarization double ratio to be much smaller than the anticipated statistical uncertainties.

Experiment 89-019 estimated systematic uncertainties on the polarization transfer observables P'_x and P'_z for proton momenta relevant for this proposal to be in the range 0.01 – 0.03, for the induced polarization P_y about 0.03. The determination of P_y is mainly limited by the knowledge of false asymmetries. The much higher statistics of the proposed measurement allow for further systematic studies and a decrease of the systematic uncertainties appears likely.

4.4. Study of the experimental sensitivity

We have shown that polarization transfer is sensitive to: spinor distortions, choice of current operator, MEC/IC, and medium modifications of the nucleon form factor. Each of these affects the two p-shells differently and has a different missing momentum dependence. The combination of both states and missing momenta provides much more stringent constraints on the models than a single point. The s-shell knockout will provide additional constraints.

We can demonstrate our ability to disentangle the various effects quantitatively in the following way. In Fig. 12, we show a sample of a χ^2 fit to sample data, generated for the positive and negative kinematical settings and two missing momentum bins per setting; only the $1p_{1/2}$ and $1p_{3/2}$ knockout were considered. The full relativistic calculation with $cc2$ current operator and wave function and optical potential as in Ref. [1] has been chosen as reference model. Then the expectation values of χ^2 per degree of freedom (d.o.f.) were calculated for different model assumptions assuming the reference calculation data and its projected standard deviations. (Thus, we expect a χ^2/d.o.f. of unity for the reference model). The different calculations compared in Fig. 12 used the positive energy projection (1–8), the full calculation (9–16) and the full calculation including medium modification of the nucleon form factor (17–24). Odd numbers refer to calculations using the $cc1$ current operator, even numbers refer to $cc2$. In each group the same combination of two different bound-state wave functions and two different optical potentials were used, which are the

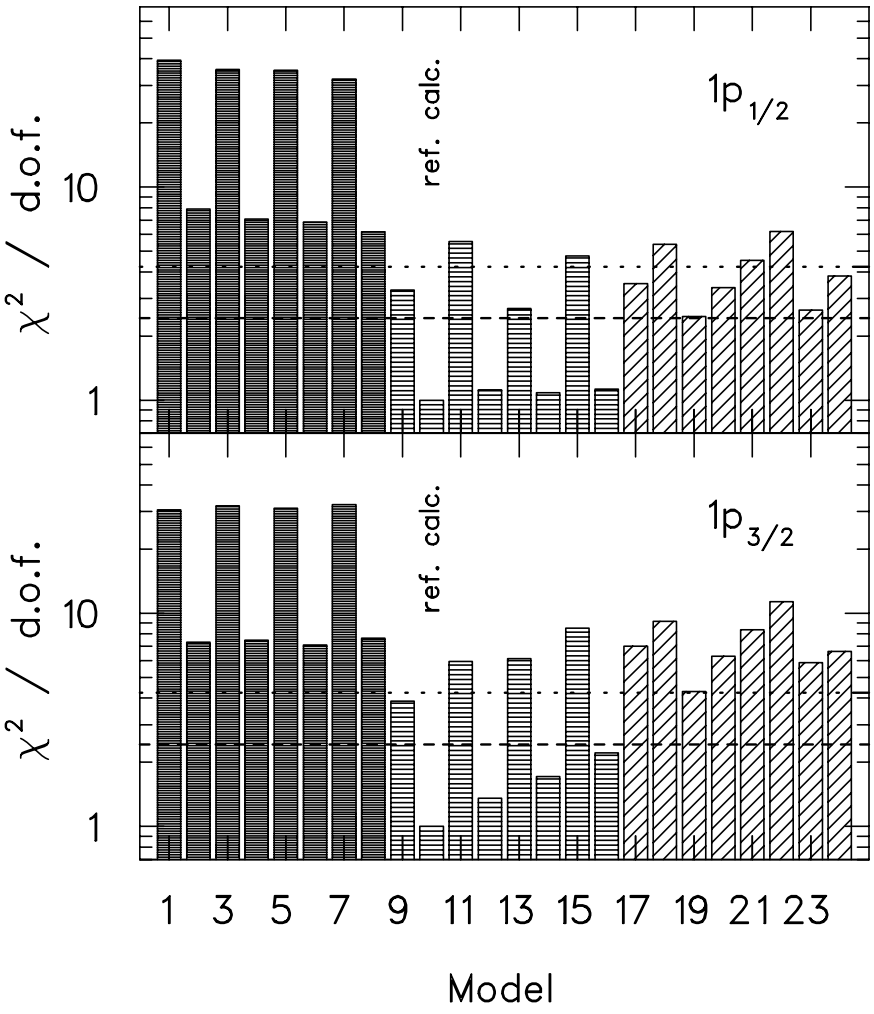

Figure 12. Experimental sensitivity for a separate analysis of the expected $1p_{1/2}$ and $1p_{3/2}$ data and a ten day running time at both positive and negative missing momentum. The expectation values of χ^2 per degree of freedom for different models are shown in logarithmic scale assuming the full calculation with $cc2$ current operator as reference. Calculations used the positive energy projection (1–8), the full calculation (9–16) and the full calculation including medium modification of the nucleon form factor (17–24). Odd numbers refer to calculations using the $cc1$ current operator, even numbers refer to $cc2$. In each group the same combination of two different bound state wave functions and two different optical potentials were used. The dashed line indicates a 4.6% confidence level, the dotted line 0.2%.

NLSH wave function used in Ref. [1] and a more recent version, fine-tuned by Udias to reproduce the low-p experiments of Leuschner *et al.* [37], and the EDAIO and EDAD2 optical potential of Cooper *et al.* [33]. Figure 12 also demonstrates the insensitivity of the polarization ratio to the particular choice of wave function and optical potential. For example, note the similarity of the χ^2/d.o.f. for models 10, 12, 14, and 16.

4.5. Beam time request

Our beam time request is based on the goal of distinguishing the three considered calculations (projected, fully relativistic, and fully relativistic including medium modified form factors) for different combinations of current operators, bound-state wave functions and optical potentials using the polarization transfer data for each of the two p-shell states separately on a confidence level corresponding to at least 2σ; the dashed lines in Fig. 12. This results in a request of 10 days of beam time at kinematics A ($p_m < 0$) and 10 days at kinematics B ($p_m > 0$). The larger effects in the s-shell knockout make a 4 day measurement in the parallel kinematics C sufficient.

A two day measurement with hydrogen provides sufficient statistical precision to determine the hydrogen polarization ratio comparable to the statistical precision of the oxygen measurement, and to make a detailed study of instrumental asymmetries.

Our beam time request is thus 27 days. The breakdown is shown in Table 9.

Table 9
Beam-time request

Purpose	Kin	Time (days)
Production data on ^{16}O	A	10
Production data on ^{16}O	B	10
Production data on ^{16}O	C	4
Production data on ^{1}H	C	2
Møller measurements, setup		1
Total		27

Acknowledgment

We gratefully acknowledge the assistance of J.M. Udias and J. Ryckebusch with theoretical calculations.

REFERENCES

1. J. Gao *et al.*, Phys. Rev. Lett. **84**, 3265 (2000).
2. N. Liyanage *et al.*, Submitted to Phys. Rev. Lett. LANL preprint nucl-ex/0009017.
3. S. Dieterich *et al.*, submitted to Phys. Lett. B., LANL preprint nucl-ex/0011008.
4. JLab expt. E93-049, R. Ent, P.Ulmer, co-spokespersons.

5. M.K. Jones *et al.*, Phys. Rev. Lett. **84**, 1398 (2000).
6. S. Malov *et al.*, Phys. Rev. C **62**, 057302 (2000).
7. D.H. Lu *et al.*, Nucl. Phys. **A634**, 443 (1998); D.H. Lu *et al.*, Phys. Lett. B **417**, 217 (1998); D.H. Lu *et al.*, Phys. Rev. C **60**, 068201 (1999).
8. J.M. Udias and J.R. Vignote, Phys. Rev. C **62**, 034302 (2000).
9. J.M. Udias, J.A. Caballero, E. Moya de Guerra, J.E. Amaro and T.W. Donnelly, Phys. Rev. Lett. **83**, 5451 (1999).
10. J.A. Caballero, T.W. Donnelly, E. Moya de Guerra, and J.M. Udias, Nucl. Phys. **A632**, 323 (1998).
11. J. Ryckebusch, D. Debruyne, W. Van Nespen, and S. Janssen, Phys. Rev. C **60**, 034604 (1999).
12. J.J. Kelly, Phys. Rev. C **60**, 044609 (1999).
13. A.W. Thomas, private communication.
14. JLab expt. E89-033, C. Chang, C. Glashausser, S. Nanda, P. Rutt, co-spokespersons.
15. JLab expt. E89-003, W. Bertozzi, K. Fissum, A. Saha, L. Weinstein, co-spokespersons.
16. JLab expt. E00-102, W. Bertozzi, K. Fissum, A. Saha, L. Weinstein, co-spokespersons.
17. K.I. Blomqvist *et al.*, Z. Phys. A **351**, 353 (1995).
18. T. de Forest, Jr., Nucl. Phys. **A392**, 232 (1983).
19. J. Ryckebusch, private communication.
20. J.M. Udias, private communication.
21. G. Brown and M. Rho, Phys. Lett. B **222**, 324 (1989).
22. Ulf-G. Meissner, Phys. Rev. Lett. **62**, 1013 (1989).
23. I.T. Cheon and M.T. Jeong, J. Phys. Soc. Jpn. **61**, 2726 (1992).
24. M.R. Frank, B.K. Jennings and G.A. Miller, Phys. Rev. C **54**, 920 (1996).
25. A. Zghiche *et al.*, Nucl. Phys. **A572**, 513 (1994).
26. R. Schiavilla, V.R. Pandharipande and A. Fabrocini, Phys. Rev. C **40**, 1484 (1989).
27. J.E. Ducret *et al.*, Nucl. Phys. **A556**, 373 (1993).
28. J. Jourdan, Nucl. Phys. **A603**, 117 (1996).
29. I. Sick, Comm. Nucl. Part. Phys. **18**, 109 (1988).
30. D.B. Day *et al.*, Ann. Rev. Nucl. Part. Sci. **40**, 357 (1990).
31. D.B. Day *et al.*, Phys. Rev. Lett. **59**, 427 (1987).
32. A.I. Akhiezer and M.P. Rekalo, Sov. J. Part. Nucl. **4**, 277 (1974); R. Arnold, C. Carlson and F. Gross, Phys. Rev. C **23**, 363 (1981).
33. E.D. Cooper *et al.*, Phys. Rev. C **47**, 297 (1993).
34. M.M. Sharma, M.A. Nagarajan, and P. Ring, Phys. Lett. B **312**, 377 (1993).
35. P. Ulmer, MCEEP, Monte Carlo for Electro-Nuclear Coincidence Experiments, Program Version 3.4, 2000.
36. J.P. Jeukenne and C. Mahaux, Nucl. Phys. **A394**, 445 (1983).
37. M. Leuschner *et al.*, Phys. Rev. C **49**,955 (1994).
38. J.W. Lightbody and J.S. O'Connell, *Computers in Physics*, May/June 1988, p. 57.
39. Hall-A status report, 2000.
40. A. Afanasev, private communication.